

MyoMapNet: Accelerated Modified Look-Locker Inversion Recovery Myocardial T₁ Mapping via Neural Networks

Hossam El-Rewaidy^{1,2}, Rui Guo¹, Amanda Paskavitz¹, Tuyen Yankama¹, Long
Ngo¹, Bjoern Menze^{2,3}, Reza Nezafat¹

¹Department of Medicine, Cardiovascular Division, Beth Israel Deaconess Medical Center and
Harvard Medical School, Boston, Massachusetts, USA

²Department of Computer Science, Technical University of Munich, Munich, Germany

³Department for Quantitative Biomedicine, University of Zurich, Switzerland

Running title: Fast MOLLI T₁ Mapping

Word Count: 4700

Address for correspondence: Reza Nezafat, PhD

Department of Medicine, Beth Israel Deaconess Medical Center,

330 Brookline Avenue, Boston, MA 02215

Phone: +1- 617-667-1747; Fax: +1- 617-975-5480

E-mail: rnezafat@bidmc.harvard.edu

Abstract

Purpose: To develop and evaluate MyoMapNet, a rapid myocardial T_1 mapping approach that uses neural networks (NN) to estimate voxel-wise myocardial T_1 and extracellular (ECV) from T_1 -weighted images collected after a single inversion pulse over 4-5 heartbeats.

Method: MyoMapNet utilizes a simple fully-connected NN to estimate T_1 values from 5 (native) or 4 (post-contrast) T_1 -weighted images. Native MOLLI-5(3)3 T_1 was collected in 717 subjects (386 males, 55 ± 16.5 years) and post-contrast MOLLI-4(1)3(1)2 in 535 subjects (232 male, 56.5 ± 15 years). The dataset was divided into training (80%) and testing (20%), where 20% of the training set was used to optimize MyoMapNet architecture (size and loss functions). We used MyoMapNet to estimate T_1 and ECV maps with the first 5 (native) or 4 (post-contrast) T_1 -weighted images from the corresponding MOLLI sequence compared to the conventional and an abbreviated MOLLI using similar number of T_1 -weighted images with 3-parameter curve-fitting.

Results: In our preliminary optimization step, we determined that a 5-layers NN trained using mean-absolute-error loss yields lower estimation errors and was used subsequently in independent testing study. The myocardial T_1 by MyoMapNet was similar to MOLLI (1200 ± 45 ms vs. 1199 ± 46 ms; $P=0.3$ for native T_1 , and $27.3 \pm 3.5\%$ vs. $27.1 \pm 4\%$; $P=0.4$ for ECV). MyoMapNet had significantly smaller errors in T_1 estimations compared to abbreviated-MOLLI (1 ± 17 ms vs. 31 ± 34 ms, $P < 0.01$ for in native T_1 , and $0.1 \pm 1.3\%$ vs. $1.9 \pm 2.5\%$, $P < 0.01$ for ECV). The duration of T_1 estimation was approximately 2 ms per slice using MyoMapNet.

Conclusion: MyoMapNet T_1 mapping enables myocardial T_1 quantification in 4-5 heartbeats with near-instantaneous map estimation time with similar accuracy and precision as MOLLI.

Keywords: Myocardial T_1 mapping, MOLLI, T_1 reconstruction, Neural network, Deep Learning.

Introduction

Cardiovascular magnetic resonance (CMR) myocardial T_1 and extracellular volume (ECV) mapping allow for non-invasive quantification of interstitial diffuse fibrosis (1). Over the past decade, there have been significant advances in CMR pulse sequences for myocardial T_1 mapping (2–11). These sequences are based on the application of magnetization preparation pulses (such as inversion (2,4,6), saturation (3,5), or a combination of both (8)) for the collection of a series of T_1 weighted images. Subsequently, tissue relaxation times are estimated using a two or three-parameter fitting model (2–12). For each of these sequences, there are different trade-offs in accuracy, precision, coverage (2D vs. 3D), and respiratory motion (free breathing vs breath-holding) (11,13–23). Alternatively, recent approaches, such as combined T_1 and T_2 mapping (21,24–27), MR fingerprinting (28,29), or multitasking (30), have been introduced to simultaneously measure different tissue parameters.

Among different myocardial T_1 mapping sequences, Modified Look-Locker (LL) inversion recovery (MOLLI) (2), acquired within a single breath-hold, is the most widely used sequence for myocardial T_1 mapping. This sequence consists of three sets of LL experiments with 3 heartbeats (or 3 seconds) in between for magnetization recovery. This acquisition is commonly referred to as the 3(3)3(3)5 MOLLI scheme, which indicates that 3, 3, and 5 images are acquired in three LL experiments with 3 rest heartbeats (i.e., 3RR interval) between each LL experiment. MOLLI-5(3)3 and MOLLI-4(1)3(1)2 were implemented to improve acquisition efficiency and precision (13,31). A variation of these sequences in which the rest period between acquisition utilizes a fixed time (1-3 second) instead of heartbeats was also implemented (32). These modifications reduce the duration of the original MOLLI from approximately 17 heartbeats to 11 heartbeats (13). In this approach, T_1 -weighted images are acquired at multiple points throughout the recovery curve, and

a pixel-wise curve fitting algorithm using a 3-parameter model is applied to estimate the T_1 values at each pixel. Recently, the inversion group (IG) fitting has also been proposed for MOLLI with shorter waiting periods between LL experiments, albeit with a penalty on precision (33–35). For shortened MOLLI (ShMOLLI) with a 5(1)1(1)1 scheme (4), a conditional fitting algorithm is utilized to discard the latter measurements for long T_1 at high heart-rates.

Alternatives to standard curve-fitting techniques in parametric mapping include dictionary-based reconstruction, simulated signal recovery, or machine learning (10,36–39). Shao et al. used a deep learning model for rapid and accurate calculation of myocardial T_1 and T_2 in Bloch equation simulation with slice profile correction (36). Similarly, Hamilton et. al. used deep learning to rapidly reconstruct T_1 and T_2 maps from CMR fingerprinting images (37). To reduce motion artifacts and minimize the acquisition window in T_1 mapping during the cardiac cycle, a convolutional neural network (CNN) model was used to reconstruct highly accelerated T_1 weighted images in slice-interleaved T_1 mapping sequences with radial sampling (38). Deep learning neural networks were also recently used to combine saturation recovery and inversion data to improve T_1 mapping precision (40). These studies have demonstrated the potential for machine learning to improve myocardial tissue characterization by increasing precision and reconstruction speed, or decreasing motion sensitivity or other confounders of T_1 mapping.

In this study, we sought to develop and evaluate a fully connected neural network (MyoMapNet)-based rapid myocardial T_1 mapping approach using a single LL experiment with a scan duration of 4-5 heartbeats and near-instantaneous (~ 2 ms) reconstruction time. The proposed MyoMapNet was trained and validated using numerically simulated data and in-vivo images; MyoMapNet's performance was compared to MOLLI with a 3-parameter fitting model.

Methods

MyoMapNet T_1 Mapping

The data acquisition for MyoMapNet is very similar to MOLLI sequence and is based on the collection of 5 (native) or 4 (post-contrast) T_1 weighted images after a single inversion pulse. **Figure 1** shows the pulse sequence and magnetization evolution of MOLLI-5(3)3 for native T_1 mapping, composed of two LL experiments to acquire eight T_1 weighted images over 11 heartbeats. In MyoMapNet, we use the five images sampled after the first inversion pulse for native MOLLI-5(3)3 T_1 measurement. For post-contrast T_1 mapping, we will use only the first four images collected using MOLLI-4(1)3(1)2 T_1 (**Supplementary Figure S1**). In contrast to MOLLI, where a 3-parameter fit model is used to estimate native or post-contrast T_1 mapping, in MyoMapNet, we propose to use a neural network to estimate T_1 values from only 5 (native) or 4 (post-contrast) T_1 images, thereby reducing the scan time to only 5 heartbeats for native and 4 heartbeats for post-contrast scans.

Numerical simulation

MOLLI-5(3)3 simulations were performed to generate the training and testing signal-intensity time courses. A single-shot readout for two sequences was simulated using Bloch equation with the following parameters: balanced Steady-State Free Precession (bSSFP) acquisition with 5 ramp-up pulses, TR/flip angle = 2.5 ms/35°, 80 phase-encode lines, acquisition window = 200 ms, and linear phase ordering. The time between the inversion and the center of k-space was 120 ms and 200 ms

for two LL experiments of MOLLI-5(3)3. Simulated T_1 ranged from 400 ms to 1800 ms with an increment of 0.1 ms, T_2 of 42 ms, and a fixed heart rate of 60 bpm. Subsequently, different Gaussian noise levels were added to the simulated signals for SNRs of 20, 40, and 100. This process was repeated 5 times for each SNR to generate a total of 80,000 signal time-courses, each with 8 time-points, to serve as data augmentation. A 3-parameter fitting model was used to calculate T_1 of each signal time course:

$$s(TI) = A - B e^{-TI/T_1^*} \quad [1]$$

where TI represents the inversion time, and A, B, and T_1^* were three unknowns. T_1 was determined from the resulting A, B, and T_1^* by applying the equation: $T_1 = T_1^* (B/A - 1)$.

In-vivo data

The study protocol was approved by the Institutional Review Board and written consent was waived. T_1 mapping data was collected as part of the clinical exam in all participants, and we retrospectively extracted T_1 mapping data. Patient data were handled in compliance with the Health Insurance Portability and Accountability Act. Imaging was performed using a 3T scanner (MAGNETOM Vida, Siemens Healthineers, Erlangen, Germany) equipped with body and spine phased-array coils.

T_1 mapping using MOLLI was collected in 717 subjects (386 males, 55 ± 16.5 years) with a subset of 535 subjects (232 males, 56.5 ± 15 years) having both native and post-contrast T_1 maps. All data were extracted retrospectively from patients who were referred for a clinical CMR exam for various cardiovascular indications from October 2018 to March 2020.

MOLLI-5(3)3 and MOLLI-4(1)3(1)2 were performed using the following parameters: bSSFP with 5 ramp-up excitations, FOV = 360×320 mm², voxel size = 1.7×1.7×8 mm³, TR/TE = 2.5 ms/1.03 ms, flip angle = 35°, linear phase-encoding ordering, partial Fourier factor = 7/8, GRAPPA acceleration factor of 2 with 24 reference lines, acquisition window ~218 ms during diastole, slice gap 12 mm. Three slices in the short-axis view (SAX) were collected in three separate breath-holds with 10 second rest periods between breath-holds. Adiabatic tan/tanh inversion pulse was used. Both MOLLI-5(3)3 and MOLLI-4(1)3(1)2 used a minimum inversion time (TI) of 100 ms with a TI increment of 80 ms. For post-contrast measurement, MOLLI-4(1)3(1)2 data was collected 15-20 min after injection of Gd-DTPA at 0.1 mmol/kg (Gadavist, Bayer Pharma AG, Berlin, Germany). MOLLI-5(3)3 and MOLLI-4(1)3(1)2 T₁ were calculated using a 3-parameter curve fitting model (Equation 1).

T₁ Estimation in MyoMapNet

MyoMapNet is a fully-connected neural network that estimates T₁ maps from input T₁-weighted images. MyoMapNet input layer has $2N_t$ nodes for N_t T₁ weighted signals and their corresponding inversion times, where $N_t=5$ in the native T₁ network, and $N_t=4$ in the post-contrast T₁ network. MyoMapNet is consisted of M_l layers each of $(200 \times S)$ nodes followed by M_l layers of $(100 \times S)$ nodes each, and one layer of $(50 \times S)$ nodes; where M_l controls the depth (total number of layers) of MyoMapNet, and S is a scaling factor to control the number of trainable parameters in each layer. For example, **Figure 2** shows the MyoMapNet architecture at $M_l = 2$ and $S = 2$, where five hidden layers of 400, 400, 200, 200, 100 nodes in each layer were utilized. A leaky rectified linear unit activation function was applied after each hidden layer. MyoMapNet

parameters were empirically optimized to balance between accurate T_1 mapping estimation and avoiding the risk of overfitting. To determine the optimal network depth and size, MyoMapNet performance was validated at $M_l = 1, 2, \text{ and } 3$ and $S = 1, 2, \text{ and } 3$. The number of parameters at different depths and scales of MyoMapNet is reported in **Table S1**.

MyoMapNet was implemented in Python using the PyTorch library version 0.41. Training and validation were performed on an NVIDIA DGX-1 system equipped with 8T V100 graphics processing units (GPUs; each with 32 GB memory and 5120 cores), central processing unit (CPU) of 88 core: Intel Xeon 2.20 GHz each, and 504 GB RAM. Only 2 GPUs were considered for training and testing the proposed MyoMapNet.

MyoMapNet Training

For simulation experiments, a set of 64,000 simulated signals (80% of the whole dataset) was randomly selected at each noise level (i.e. SNR of 100, 40, and 20). Each of these datasets was used to train the MyoMapNet separately. For in-vivo studies, training datasets of 573 patients (1719 native T_1 maps) and 428 patients (1281 post-contrast T_1 maps) were randomly selected for the native and post-contrast map reconstructions, respectively. A detailed description of data splitting is included in **Supplementary Figure S2**. Corrupted native T_1 maps (249 maps) due to image artifacts were excluded from the training dataset. MOLLI-5(3)3 and MOLLI-4(1)3(1)2 T_1 maps were estimated using 8 (native) or 9 (post-contrast) T_1 -weighted images. We performed all the map reconstruction offline without motion correction. Two loss functions were studied to minimize the error between the estimated and reference MOLLI T_1 values:

a) The mean-absolute error loss function (MAE) = $\frac{1}{n} \sum_{i=1}^n |estimated_T_{1i} - MOLLI_T_{1i}|$

b) The mean-squared error loss (MSE) = $\frac{1}{n} \sum_{i=1}^n (\text{estimated_}T_{1_i} - \text{MOLLI_}T_{1_i})^2$

where n is the number of T_1 samples in a minibatch of the training dataset (batch size = 80 T_1 maps). To select the optimal loss function and network size, the training dataset was further split into subsets of 80% training and 20% validation of the network for the optimization experiments only. The stochastic gradient descent optimizer with an initial learning rate of 1E-8 and momentum of 0.8 was used to train the network for 2000 epochs with a batch size of 80 maps. The same hyperparameters were used to train all models on native and post-contrast datasets, except for networks with $S = 3$ or $M_l = 3$, where a batch size of 60 T_1 maps was used. MyoMapNet took 8.3 ± 2.5 hours to be trained using the native T_1 dataset.

MyoMapNet Evaluation

The performance of MyoMapNet was evaluated using the independent testing dataset. The simulated testing dataset contained 16,000 samples, containing T_1 ranging from 400 to 1800ms. For in-vivo studies, we used native T_1 maps from 144 patients (432 MOLLI-5(3)3 T_1 maps) and post-contrast T_1 maps from 107 patients (324 MOLLI-4(1)3(1)2 T_1 maps). For each T_1 map, we calculated 3 sets of T_1 estimates: (a) *standard MOLLI* T_1 mapping using 3-parameter curve fitting from all collected images (8, or 9 images in native or post-contrast T_1 mapping, respectively), (b) *abbreviated MOLLI* using only 5 native (MOLLI-5) or 4 post-contrast MOLLI (MOLLI-4) images using standard 3-parameter curve fitting, and (c) *MyoMapNet* using only 5 native or 4 post-contrast T_1 weighted images, retrospectively extracted from the standard MOLLI dataset. The ECV values were calculated for patients who had both native and post-contrast T_1 mapping available in the testing dataset (75 patients).

Data analysis

Endocardial and epicardial contours were drawn to measure global T_1 values. **Supplementary Figure S3** shows example contours for 4 different subjects. The mean and standard deviation of T_1 or ECV from the LV myocardium were calculated. The global T_1 was measured by averaging the myocardial T_1 from three different slices. Native, post-contrast T_1 , and ECV values were reported as mean \pm standard deviation. The 95% confidence interval (95% CI) of the mean was reported to represent a range of values that contains the true mean of the population with 95% certainty. The precision of T_1 maps was assessed using the standard deviation of T_1 values within the myocardium. Bland-Altman analysis was used to characterize per slice and per patient T_1 estimated by two different methods (abbreviated MOLLI vs. standard MOLLI, and MyoMapNet vs. standard MOLLI) and reported as the mean difference of T_1 estimations and 95% limits of agreements.

Group differences in per-slice T_1 measurements were assessed using linear mixed-effects models with compound symmetry covariance structure (41). In these models, the pair-wise group difference was fitted as the outcome, and the subject was included as a random intercept. The average and standard deviation of T_1 were compared between two methods using the paired Student's t-test. Bonferroni correction was utilized to account for three pair-wise group comparisons. All tests were two-sided and the nominal level of statistical significance was 0.0167.

Results

Network optimization

The native T_1 estimation errors between MyoMapNet and standard MOLLI-5(3)3 in the validation dataset at different loss functions, number of layers, and number of nodes per layer (18 networks in total) are summarized in **Table 1**. In general, MAE loss showed consistently lower errors than MSE at different network sizes and was therefore used to train all MyoMapNet models. For MAE, small changes in T_1 estimation errors were reported between MyoMapNet and MOLLI-5(3)3 at different network sizes with slightly lower STD for bigger networks. MyoMapNet of 5 hidden layers ($M_l = 2$) and 400, 400, 200, 200, and 100 nodes ($S = 2$) at each layer with a total of 305,401 trainable parameters, was therefore used for all T_1 estimation models to balance between small estimation errors and lower chances of overfitting due to increased number of parameters.

Numerical Simulations

Figure 3 shows the differences in estimated T_1 between the MOLLI-5 (left) and MyoMapNet (right) vs MOLLI-5(3)3, simulated at SNR levels of 100, 40, and 20. For higher SNR, the estimated T_1 values using MOLLI-5 exhibit a systematic error as a function of T_1 values. For the same SNR, MyoMapNet shows no systematic error for different T_1 values. As SNR decreases, there is an increase in the error of estimated T_1 values using both techniques, but with lower error in MyoMapNet (0 ± 15 ms, 95% CI [-0.3, 0.1]) compared to MOLLI-5 (-3 ± 32 ms, and 95% CI [-4, -3]; $P < 0.001$) relative to MOLLI-5(3)3 at SNR=40. At SNR=20, the mean difference between MyoMapNet and MOLLI-5(3)3 was (0 ± 31 ms, 95% CI [-1, 1]) compared to MOLLI-5 (-3 ± 54 ms, 95% CI [-4, -3]; $P < 0.001$).

In-vivo Studies:

Figure 4 shows example native T_1 maps reconstructed with the MOLLI-5(3)3, MOLLI-5, and MyoMapNet in four subjects. The T_1 maps using MyoMapNet showed sharp myocardial T_1 boundaries with more homogeneous T_1 estimations similar to that of MOLLI-5(3)3 maps when compared to the MOLLI-5 method. This inhomogeneity in MOLLI-5 T_1 estimations is more apparent in the blood pool, affecting the accuracy and precisions of the estimated T_1 values.

The mean T_1 values and precision for myocardial native and post-contrast T_1 , and ECV maps are summarized in **Table 2**. MyoMapNet yields T_1 and ECV values similar to those of the standard MOLLI methods with lower estimation errors compared to abbreviated MOLLI methods (1230 ± 63 , 1200 ± 45 , and 1199 ± 46 ms for native T_1 values; 548 ± 63 , 563 ± 45 , and 565 ± 47 ms for post-contrast T_1 , and 29.3 ± 5.6 , 27.3 ± 3.5 , and $27.1\pm 4\%$ for ECV values using abbreviated MOLLI, MyoMapNet, and standard MOLLI methods, respectively). For native T_1 precision, the average precision of MyoMapNet T_1 estimations (120 ms, 95% CI [117, 122]) was superior to MOLLI-5 (148 ms, 95% CI [144, 151]; $P < 0.01$) and inferior to standard MOLLI-5(3)3 (112 ms, 95% CI [109, 114]; $P < 0.01$). In post-contrast T_1 , the average precision of MyoMapNet T_1 estimations (44 ms, 95% CI [42, 45]) was similar to the standard MOLLI-4(1)3(1)2 (43 ms, 95% CI [41, 44]; $P = 0.05$) and significantly higher than MOLLI-4 (52 ms, 95% CI [50, 54]; $P < 0.01$).

Bland-Altman plots for T_1 , post-contrast T_1 , and ECV for three different approaches (**Figure 5**) show similar measurements for MyoMapNet when compared to MOLLI, with increased measurement error for abbreviated MOLLI. Similar results were observed for per slice analysis of the three methods (**Supplementary Figure S4**).

The duration for estimating T_1 maps was 24.2 ± 0.5 sec by a 3-parameter fitting model without motion correction using Matlab on CPU, and 2 ± 0.01 ms by MyoMapNet using Python on GPU.

Discussion

In this study, we evaluated the potential of a fully connected neural network for native and post-contrast myocardial T_1 and ECV mapping from 4-5 T_1 weighted images, reducing the scan time of myocardial T_1 mapping by 50% without compromising accuracy or precision.

Respiratory motion in myocardial tissue mapping causes artifacts that adversely impact the quantification of tissue relaxation times. To minimize respiratory motion artifacts, imaging during breath-holding or use of respiratory slice tracking have been used (6,42–48). For MOLLI, images for each slice are collected in a single breath-hold. However, even with breath-holding, patients often have respiratory motion-induced drift, which creates artifacts in maps. Therefore, respiratory motion correction is still being recommended (1). Similarly, for free-breathing tissue characterization, while slice tracking reduced through-plane motion, motion correction is necessary to align images (44,46). Furthermore, motion correction will improve the reproducibility and robustness of tissue mapping (49). One of the advantages of MyoMapNet is reducing the sensitivity to respiratory motion. **Supplementary Figure S5** shows example images demonstrating the presence of motion in standard MOLLI data, despite breath-holding. In this study, we used retrospectively collected data and were not able to perform a head-to-head comparison of the impact of shorter scan time on the motion. Further studies are warranted to further investigate the potential advantages of MyoMapNet in reducing motion sensitivity.

The numerical simulations of native T_1 MOLLI with SNR=100 showed systematic errors as a function of the T_1 value increments associated with MOLLI-5 relative to the standard MOLLI-5(3)3 estimations. The MyoMapNet learns a correction function to minimize such systematic errors and create unbiased T_1 estimations at different ranges of T_1 values. As more noise was added to the T_1 -weighted signals, the MOLLI-5 exhibited higher T_1 estimation errors. MyoMapNet significantly reduces the errors associated with noise, while correcting for systematic errors. Similar observations were seen in the in-vivo data for native and post-contrast T_1 mapping, where MyoMapNet showed significantly lower T_1 and ECV estimation errors compared to the abbreviated MOLLI methods.

Machine learning is rapidly improving the workflow of myocardial tissue characterization in CMR (50). Recent studies have demonstrated the potential for deep learning in automating analysis workflow and quality control (39,51,52). These methods could automatically perform motion correction, segmentation, and parameter quantification, thereby reducing the burden and observer-related variability of manual analysis. The MyoMapNet could be easily integrated with an automated analysis and quality control method to simplify the workflow.

In this study, we reduced the number of T_1 -weighted images to 4-5 images for estimating T_1 values without rigorously studying the impact of the number of T_1 -weighted images. Further studies are warranted to investigate the optimal number of T_1 -weighted images for myocardial T_1 mapping. For MOLLI, after LL, samplings along the relaxation curve are separated by cardiac cycle. The choice of inversion time can potentially impact the accuracy and precision of tissue mapping (53). Hence, the effective LL times are determined by the RR interval length. In a single LL experiment, only the first T_1 -weighted image has a short LL time ($<RR$ interval length), while the rest of the images have a long LL time and hence are less sensitive to T_1 . This is more prominent in post-

contrast T_1 mapping where T_1 times range from 100 to 600 ms, which will impact the quality of the T_1 map. Other acquisition schemes, such as 4(1)1 for native T_1 , or 3(1)1 or 2(1)2 for post-contrast T_1 , could add another LL anchor at the beginning of the relaxation curve to increase the susceptibility of T_1 , without increasing the scan time more, which necessitates further investigation.

The fully-connected neural network architecture adopted in MyoMapNet was more convenient for the pixel-wise, short, fixed-length input data (10 in native or 8 in post-contrast T_1 MOLLI) than convolutional-based neural networks to learn features from all combinations of the input data with a maximum receptive field. Similar fully-connected based architectures were utilized for simultaneous calculation of T_1 and T_2 maps from MR fingerprinting acquisitions in cardiac and brain imaging (37,54). On the other hand, a one-dimensional convolutional neural network was used to estimate T_1 and T_2 maps from a relatively longer input of 220 signal intensity values and inversion time stamps of BLESSPC acquisitions (36). Other architectures for MyoMapNet can be investigated for T_1 estimations in future studies. MyoMapNet was also successful in estimating T_1 values in two MOLLI sequences, MOLLI-5(3)3, and MOLLI-4(1)3(1)2, which indicates its flexibility and potential generalizability to other T_1 and T_2 sequences. Future studies are warranted to investigate the generalizability of MyoMapNet to alternative T_1 and T_2 sequences.

Our study has several limitations. MyoMapNet was validated using retrospectively acquired data derived from standard MOLLI-5(3)3 and MOLLI-4(1)3(1)2, instead of collecting dedicated data with 4-5 T_1 -weighted images. We only evaluated MyoMapNet using MOLLI data, a similar concept can be investigated for other T_1 mapping sequences. We did not perform any motion correction in T_1 mapping. We used MOLLI sequence for training, and it is widely known that MOLLI has intrinsic under-estimation. Further studies should be pursued to investigate the potential of MyoMapNet to improve measurement accuracy. We used a large dataset of patients

with different clinical indications, therefore the clinical utility of MyoMapNet was not studied. Finally, data from a single vendor and field strength was used for training and the generalizability of the trained network for other field strengths or MR vendor should be studied.

Conclusion

The MyoMapNet enables fast and precise myocardial T_1 mapping quantification from only 4-5 T_1 -weighted images acquired after a single look-locker sequence, leading to shorter scan time and rapid map reconstruction.

Funding Information

Reza Nezafat receives grant funding by the National Institutes of Health (NIH) 1R01HL129185, 1R01HL129157, 1R01HL127015 and 1R01HL154744 (Bethesda, MD, USA); and the American Heart Association (AHA) 15EIA22710040 (Waltham, MA, USA). All other authors have reported that they have no relationships relevant to the contents of this paper to disclose.

Data Availability Statement

The codes of MyoMapNet are openly available in Harvard dataverse at <https://dataverse.harvard.edu/dataverse/cardiacmr>, reference number (https://doi.org/10.7910/DVN/VYV31B).

References

1. Messroghli DR, Moon JC, Ferreira VM, et al. Clinical recommendations for cardiovascular magnetic resonance mapping of T1, T2, T2* and extracellular volume: A consensus statement by the Society for Cardiovascular Magnetic Resonance (SCMR) endorsed by the European Association for Cardiovascular Imaging (EACVI). *J. Cardiovasc. Magn. Reson.* 2017;19:75.
2. Messroghli DR, Radjenovic A, Kozerke S, Higgins DM, Sivananthan MU, Ridgway JP. Modified Look-Locker inversion recovery (MOLLI) for high-resolution T1 mapping of the heart. *Magn. Reson. Med.* 2004;52:141–146.
3. Chow K, Flewitt JA, Green JD, Pagano JJ, Friedrich MG, Thompson RB. Saturation recovery single-shot acquisition (SASHA) for myocardial T1 mapping. *Magn. Reson. Med.* 2014;71:2082–2095.
4. Piechnik SK, Ferreira VM, Dall'Armellina E, et al. Shortened Modified Look-Locker Inversion recovery (ShMOLLI) for clinical myocardial T1 mapping at 1.5 and 3 T within a 9 heartbeat breathhold. *J. Cardiovasc. Magn. Reson.* 2010;12:69.
5. Fitts M, Breton E, Kholmovski EG, et al. Arrhythmia insensitive rapid cardiac T1 mapping pulse sequence. *Magn. Reson. Med.* 2013;70:1274–1282.
6. Weingärtner S, Roujol S, Akçakaya M, Basha TA, Nezafat R. Free-breathing multislice native myocardial T1 mapping using the slice-interleaved T1 (STONE) sequence. *Magn. Reson. Med.* 2015;74:115–124.
7. Mehta BB, Chen X, Bilchick KC, Salerno M, Epstein FH. Accelerated and navigator-gated look-locker imaging for cardiac T1 estimation (ANGIE): Development and application to T1 mapping of the right ventricle. *Magn. Reson. Med.* 2015;73:150–160.
8. Weingärtner S, Akçakaya M, Basha T, et al. Combined saturation/inversion recovery sequences for improved evaluation of scar and diffuse fibrosis in patients with arrhythmia or heart rate variability. *Magn. Reson. Med.* 2014;71:1024–1034.
9. Guo R, Cai X, Kucukseymen S, et al. Free-breathing whole-heart multi-slice myocardial T1 mapping in 2 minutes. *Magn. Reson. Med.* 2021;85:89–102.
10. Shao J, Rapacchi S, Nguyen KL, Hu P. Myocardial T1 mapping at 3.0 tesla using an inversion recovery spoiled gradient echo readout and bloch equation simulation with slice profile correction (BLESSPC) T1 estimation algorithm. *J Magn Reson Imaging* 2016;43:414–425.
11. Roujol S, Weingärtner S, Foppa M, et al. Accuracy, precision, and reproducibility of four T1 mapping sequences: A head-to-head comparison of MOLLI, ShMOLLI, SASHA, and SAPHIRE. *Radiology* 2014;272:683–689.
12. Akçakaya M, Basha TA, Weingärtner S, Roujol S, Berg S, Nezafat R. Improved quantitative myocardial T2 mapping: Impact of the fitting model. *Magn. Reson. Med.* 2015;74:93–105.
13. Kellman P, Hansen MS. T1 mapping in the heart: Accuracy and precision. *J. Cardiovasc. Magn. Reson.* 2014;16:2.
14. Nordio G, Bustin A, Henningsson M, et al. 3D SASHA myocardial T1 mapping with high accuracy and improved precision. *Magn. Reson. Mater. Physics, Biol. Med.* 2019;32:281–289.
15. Guo R, Chen Z, Herzka DA, Luo J, Ding H. A three-dimensional free-breathing sequence for simultaneous myocardial T1 and T2 mapping. *Magn. Reson. Med.* 2019;81:1031–1043.
16. Shao J, Liu D, Sung K, Nguyen KL, Hu P. Accuracy, precision, and reproducibility of myocardial T1 mapping: A comparison of four T1 estimation algorithms for modified look-locker inversion recovery (MOLLI). *Magn. Reson. Med.* 2017;78:1746–1756.
17. Weingärtner S, Akçakaya M, Roujol S, et al. Free-breathing post-contrast three-dimensional

- T1 mapping: Volumetric assessment of myocardial T1 values. *Magn. Reson. Med.* 2015;73:214–222.
18. Weingärtner S, Akçakaya M, Roujol S, et al. Free-breathing combined three-dimensional phase sensitive late gadolinium enhancement and T1 mapping for myocardial tissue characterization. *Magn. Reson. Med.* 2015;74:1032–1041.
 19. Nordio G, Henningsson M, Chiribiri A, Villa ADM, Schneider T, Botnar RM. 3D myocardial T1 mapping using saturation recovery. *J. Magn. Reson. Imaging* 2017;46:218–227.
 20. Qi H, Jaubert O, Bustin A, et al. Free-running 3D whole heart myocardial T1 mapping with isotropic spatial resolution. *Magn. Reson. Med.* 2019;82:1331–1342.
 21. Kvernby S, Warntjes MJ a. B, Haraldsson H, Carlhäll CJ, Engvall J, Ebberts T. Simultaneous three-dimensional myocardial T1 and T2 mapping in one breath hold with 3D-QALAS. *J. Cardiovasc. Magn. Reson.* 2014;16:102.
 22. Nordio G, Bustin A, Odille F, et al. Faster 3D saturation-recovery based myocardial T1 mapping using a reduced number of saturation points and denoising. *PLoS One* 2020;15.
 23. Xanthis CG, Bidhult S, Greiser A, et al. Simulation-based quantification of native T1 and T2 of the myocardium using a modified MOLLI scheme and the importance of Magnetization Transfer. *Magn. Reson. Imaging* 2018;48:96–106.
 24. Akçakaya M, Weingärtner S, Basha TA, Roujol S, Bellm S, Nezafat R. Joint myocardial T1 and T2 mapping using a combination of saturation recovery and T2-preparation. *Magn. Reson. Med.* 2016;76:888–896.
 25. Qi H, Bustin A, Cruz G, et al. Free-running simultaneous myocardial T1/T2 mapping and cine imaging with 3D whole-heart coverage and isotropic spatial resolution. *Magn. Reson. Imaging* 2019;63:159–169.
 26. Guo R, Cai X, Kucukseymen S, et al. Free-breathing simultaneous myocardial T1 and T2 mapping with whole left ventricle coverage. *Magn. Reson. Med.* 2020;85.
 27. Kvernby S, Warntjes M, Engvall J, Carlhäll CJ, Ebberts T. Clinical feasibility of 3D-QALAS – Single breath-hold 3D myocardial T1- and T2-mapping. *Magn. Reson. Imaging* 2017;38:13–20.
 28. Hamilton JI, Jiang Y, Chen Y, et al. MR fingerprinting for rapid quantification of myocardial T1, T2, and proton spin density. *Magn. Reson. Med.* 2017;77:1446–1458.
 29. Jaubert O, Cruz G, Bustin A, et al. Free-running cardiac magnetic resonance fingerprinting: Joint T1/T2 map and Cine imaging. *Magn. Reson. Imaging* 2020;68:173–182.
 30. Christodoulou AG, Shaw JL, Nguyen C, et al. Magnetic resonance multitasking for motion-resolved quantitative cardiovascular imaging. *Nat. Biomed. Eng.* 2018;2:215–226.
 31. Kellman P, Wilson JR, Xue H, Ugander M, Arai AE. Extracellular volume fraction mapping in the myocardium, part 1: evaluation of an automated method. *J Cardiovasc Magn Reson* 2012;14:63.
 32. Kellman P, Arai AE, Xue H. T1 and extracellular volume mapping in the heart: Estimation of error maps and the influence of noise on precision. *J. Cardiovasc. Magn. Reson.* 2013;15:56.
 33. Sussman MS, Yang IY, Fok KH, Wintersperger BJ. Inversion group (IG) fitting: A new T1 mapping method for modified look-locker inversion recovery (MOLLI) that allows arbitrary inversion groupings and rest periods (including no rest period). *Magn. Reson. Med.* 2016;75:2332–2340.
 34. Sussman MS, Wintersperger BJ. Modified look-locker inversion recovery (MOLLI) T1 mapping with inversion group (IG) fitting – A method for improved precision. *Magn. Reson. Imaging* 2019;62:38–45.

35. D'Errico L, Sussman MS, Hanneman K, Wintersperger BJ. Precision-optimized single protocol pre-/post-contrast modified-look locker inversion T1 mapping using composite inversion group fitting. *Magn. Reson. Imaging* 2020;74:195–202.
36. Shao J, Ghodrati V, Nguyen KL, Hu P. Fast and accurate calculation of myocardial T1 and T2 values using deep learning Bloch equation simulations (DeepBLESS). *Magn. Reson. Med.* 2020;84:2831–2845.
37. Hamilton JI, Currey D, Rajagopalan S, Seiberlich N. Deep learning reconstruction for cardiac magnetic resonance fingerprinting T1 and T2 mapping. *Magn. Reson. Med.* 2020.
38. Nezafat M, El-Rewaify H, Kucukseymen S, Hauser TH, Fahmy AS. Deep convolution neural networks based artifact suppression in under-sampled radial acquisitions of myocardial T1 mapping images. *Phys. Med. Biol.* 2020;65:225024.
39. Zhu Y, Fahmy AS, Duan C, Nakamori S, Nezafat R. Automated Myocardial T2 and Extracellular Volume Quantification in Cardiac MRI Using Transfer Learning-based Myocardium Segmentation. *Radiol Artif Intell* 2020;2:e190034.
40. Gatsoni O, Aletras AH, Heiberg E, Berggran K. T1 Mapping By Means Of Deep Learning Neural Networks Using Both Saturation Recovery and Inversion Recovery Data. In: Society for Cardiovascular Magnetic Resonance (SCMR). Orlando, FL; 2020.
41. Bates D, Mächler M, Bolker BM, Walker SC. Fitting linear mixed-effects models using lme4. *J. Stat. Softw.* 2015;67:1–48.
42. Xue H, Shah S, Greiser A, et al. Motion correction for myocardial T1 mapping using image registration with synthetic image estimation. *Magn. Reson. Med.* 2012;67:1644–1655.
43. Zhu Y, Kang J, Duan C, et al. Integrated motion correction and dictionary learning for free-breathing myocardial T1 mapping. *Magn. Reson. Med.* 2019;81:2644–2654.
44. El-Rewaify H, Nezafat M, Jang J, Nakamori S, Fahmy AS, Nezafat R. Nonrigid active shape model-based registration framework for motion correction of cardiac T1 mapping. *Magn. Reson. Med.* 2018;00:1–12.
45. Nordio G, Schneider T, Cruz G, et al. Whole-heart T1 mapping using a 2D fat image navigator for respiratory motion compensation. *Magn. Reson. Med.* 2020;83:178–187.
46. Roujol S, Foppa M, Weingärtner S, Manning WJ, Nezafat R. Adaptive Registration of Varying Contrast-Weighted Images for Improved Tissue Characterization (ARCTIC): Application to T1 Mapping. *Magn. Reson. Med.* 2015;73:1469–1482.
47. Becker KM, Blaszczyk E, Funk S, et al. Fast myocardial T1 mapping using cardiac motion correction. *Magn. Reson. Med.* 2020;83:438–451.
48. Bush MA, Pan Y, Jin N, et al. Prospective correction of patient-specific respiratory motion in myocardial T1 and T2 mapping. *Magn. Reson. Med.* 2021;85:855–867.
49. Roujol S, Basha TA, Weingärtner S, et al. Impact of motion correction on reproducibility and spatial variability of quantitative myocardial T2 mapping. *J. Cardiovasc. Magn. Reson.* 2015;17:46.
50. Leiner T, Rueckert D, Suinesiaputra A, et al. Machine learning in cardiovascular magnetic resonance: Basic concepts and applications. *J. Cardiovasc. Magn. Reson.* 2019;21.
51. Fahmy AS, El-Rewaify H, Nezafat M, Nakamori S, Nezafat R. Automated analysis of cardiovascular magnetic resonance myocardial native T1 mapping images using fully convolutional neural networks. *J Cardiovasc Magn Reson* 2019;21:1–12.
52. Zhang Q, Hann E, Werys K, et al. Deep learning with attention supervision for automated motion artefact detection in quality control of cardiac T1-mapping. *Artif. Intell. Med.* 2020;110.
53. Akçakaya M, Weingärtner S, Roujol S, Nezafat R. On the selection of sampling points for

myocardial T1 mapping. *Magn. Reson. Med.* 2015;73:1741–1753.

54. Cohen O, Zhu B, Rosen MS. MR fingerprinting Deep RecOnstruction NEtwork (DRONE). *Magn. Reson. Med.* 2018;80:885–894.

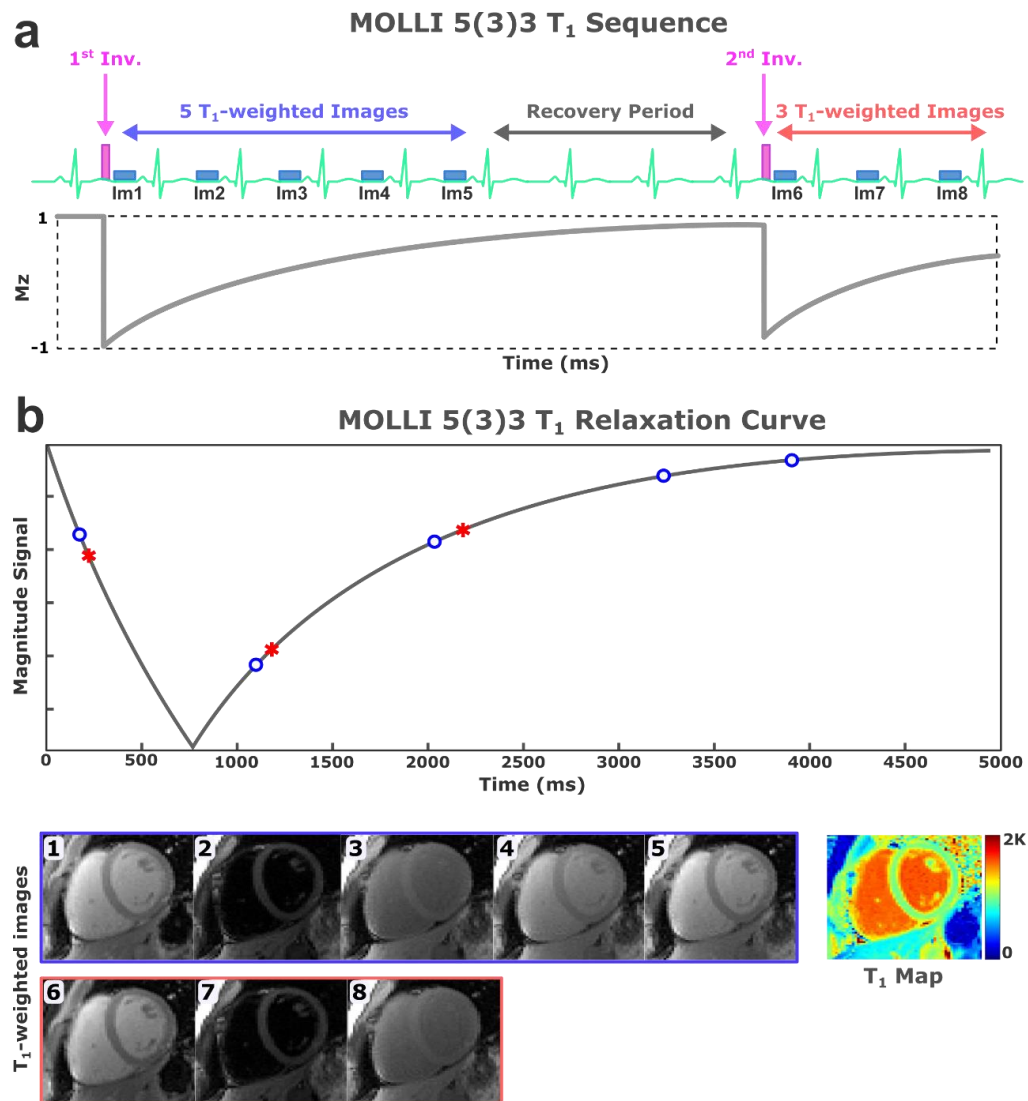


Figure 1. MOLLI-5(3)3 sequence (a) and associated signal recovery (b): two look-locker inversion pulses are performed to acquire eight T_1 -weighted images with a recovery period of 3 heartbeats between look-lockers. In MyoMapNet, images collected after the first inversion pulse are used for estimating the T_1 values.

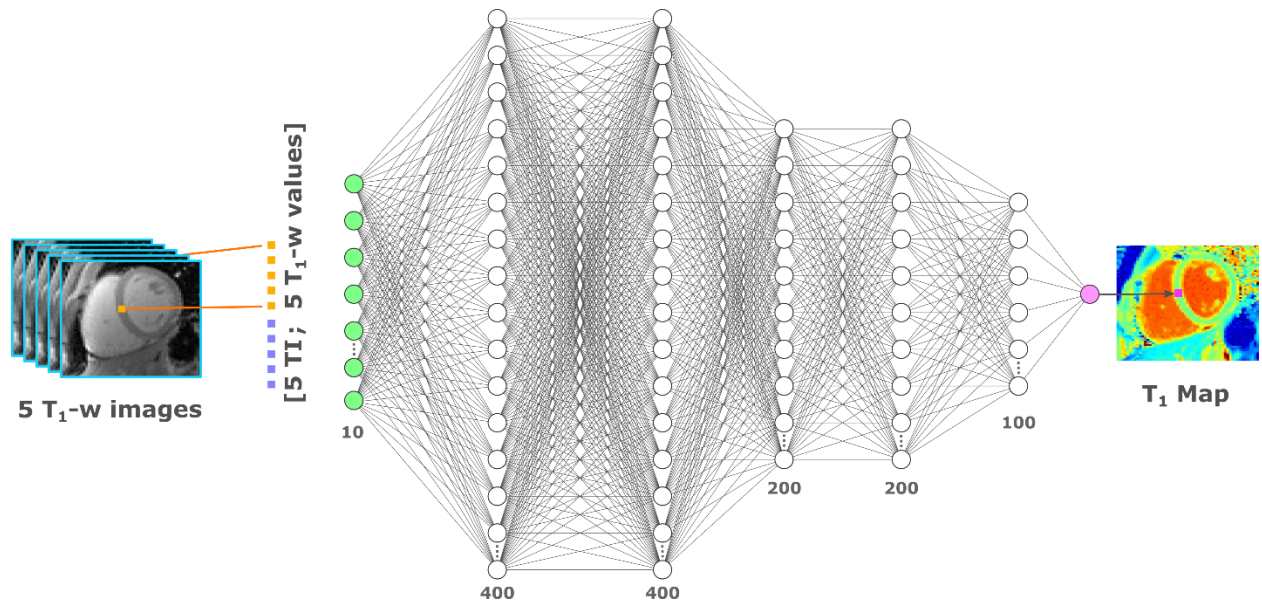


Figure 2. MyoMapNet architecture: MyoMapNet uses a fully-connected neural network for estimating pixel-wise T_1 values from T_1 -weighted images collected after a single look-locker inversion pulse (i.e. the first 5 images of MOLLI-5(3)3 or first 4 images of MOLLI-4(1)3(1)2). For each voxel, the signal values from 5 T_1 -weighted images are concatenated with their corresponding look-locker times and used as the network input (i.e. 10×1) for native T_1 mapping. The input values are fed to a fully-connected network with 5 hidden layers with 400, 400, 200, 200, and 100 nodes each layer, respectively. The output is the estimated T_1 value at each voxel.

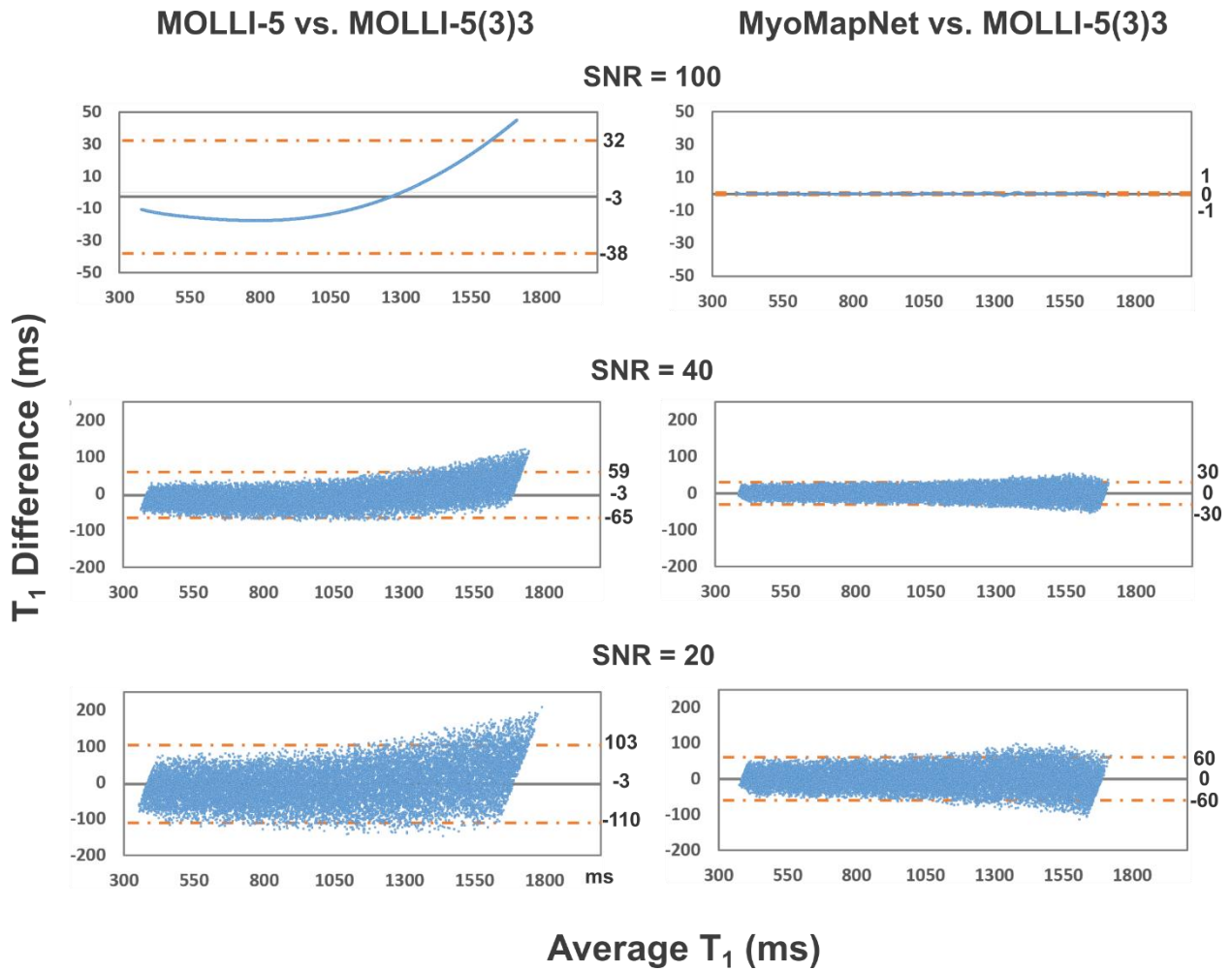


Figure 3. Bland-Altman plots showing the mean difference and 95% limits of agreement between the simulated T_1 values by the MOLLI-5 vs. MOLLI-5(3)3 (left column) and MyoMapNet vs. MOLLI-5(3)3 (right column) for SNR of 100, 40, and 20. MOLLI-5 yields a systematic error in T_1 estimations, which is corrected in MyoMapNet.

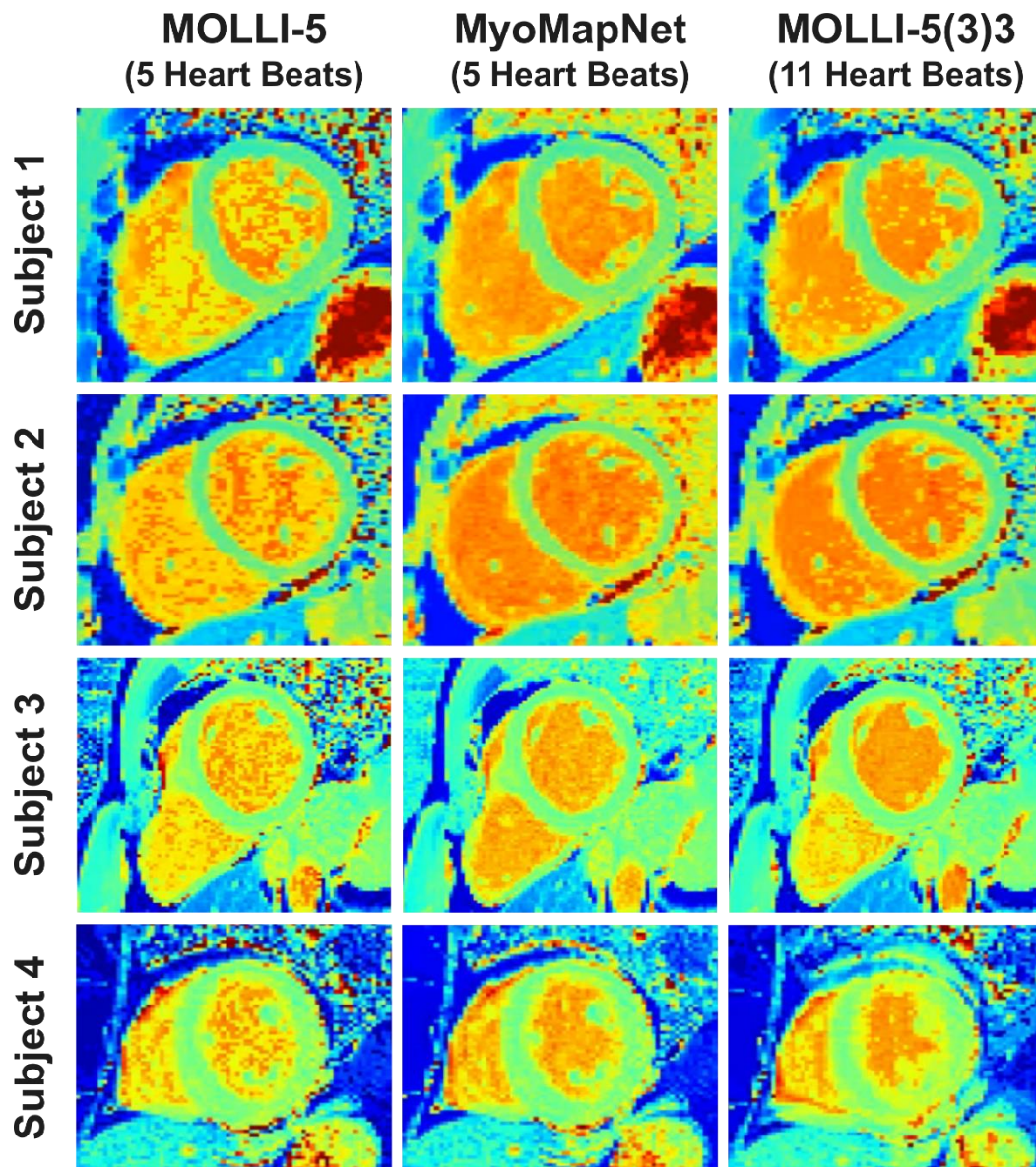


Figure 4. Native T_1 maps from four patients, reconstructed using MOLLI-5 (using only 5 T_1 weighted images with 3-parameter fitting), MyoMapNet, and MOLLI-5(3)3 with a 3-parameter fitting model. MyoMapNet yield maps with more homogenous signal compared to MOLLI-5.

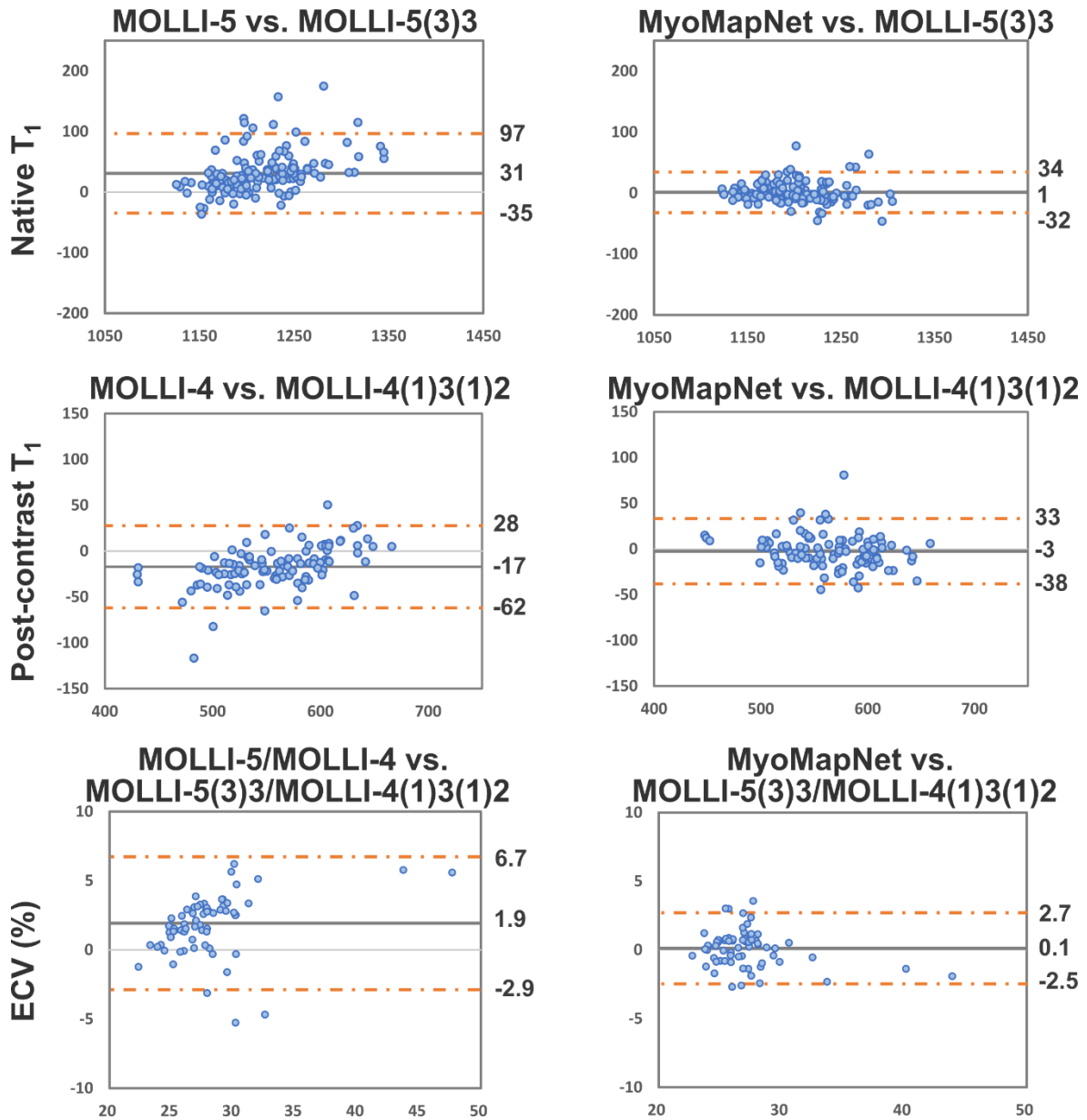


Figure 5. Bland-Altman plots showing the mean difference and 95% limits of agreement for global native, post-contrast T₁, and ECV for the abbreviated MOLLI-5/MOLLI-4 vs. standard MOLLI-5(3)3/MOLLI-4(1)3(1)2 (left column) and MyoMapNet vs. standard MOLLI-5(3)3/MOLLI-4(1)3(1)2 (right column). Each dot represents the values calculated from one patient.

Table 1. Mean difference (\pm STD) in T_1 values between MyoMapNet and MOLLI-5(3)3 at different loss functions (MSE, and MAE), network depth (3, 5, and 7 layers) and network size (S=1, 2, and 3).

| | MSE Loss | | | MAE Loss | | |
|-----|-------------|-------------|-------------|------------|------------|------------|
| | 3 layers | 5 layers | 7 layers | 3 layers | 5 layers | 7 layers |
| S=1 | 0 ± 25 | 12 ± 30 | 9 ± 24 | 3 ± 27 | 5 ± 24 | 5 ± 24 |
| S=2 | 12 ± 23 | 5 ± 24 | 5 ± 22 | 6 ± 24 | 3 ± 24 | 4 ± 22 |
| S=3 | 11 ± 23 | 18 ± 21 | -2 ± 24 | 3 ± 24 | 3 ± 23 | 3 ± 22 |

Table 2. T₁/ECV values and precision (standard deviation of measurements within myocardium) for the MOLLI-5, MyoMapNet, and MOLLI-5(3)3 in the testing dataset of 144, 107 and 75 patients for native T₁, post-contrast, and ECV, respectively.

| | Myocardial T ₁ and ECV | | | Precision | | |
|-----------------------------------------|-----------------------------------|-----------|---------------------------------|---------------------|-----------|---------------------------------|
| | MOLLI-5/ MOLLI-4 | MyoMapNet | MOLLI-5(3)3/ MOLLI-4(1)3(1)2 | MOLLI-5/ MOLLI-4 | MyoMapNet | MOLLI-5(3)3/ MOLLI-4(1)3(1)2 |
| Native T₁ (ms) | 1230 ± 63* § | 1200 ± 45 | 1199 ± 46 | 148 ± 34* § | 120 ± 27* | 112 ± 27 |
| Post-contrast T₁ (ms) | 548 ± 63* § | 563 ± 45 | 565 ± 47 | 52 ± 11* § | 44 ± 11 | 43 ± 10 |
| ECV (%) | 29 ± 6* § | 27 ± 4 | 27 ± 4 | - | - | - |

*p-value < 0.01 when compared to MOLLI.

§p-value < 0.01 when compared to MyoMapNet.

Table S1. Number of parameters at different MyoMapNet depth (3, 5, and 7 layers) and network size (S=1, 2, and 3).

| | 3 layers | 5 layers | 7 layers |
|------------|-----------------|-----------------|-----------------|
| S=1 | 27401 | 77701 | 128001 |
| S=2 | 104801 | 305401 | 506001 |
| S=3 | 232201 | 683101 | 1134001 |

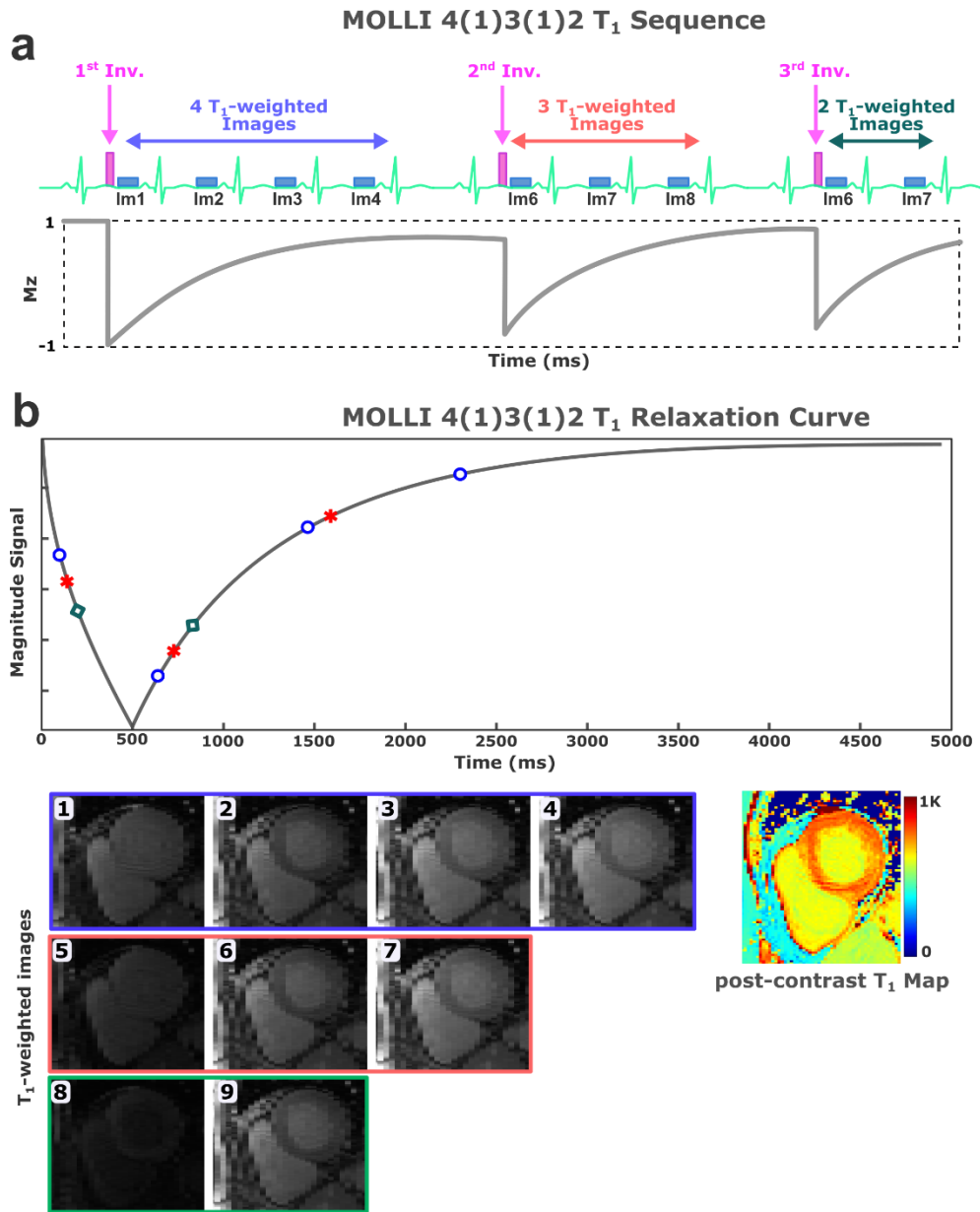


Figure S1. MOLLI-4(1)3(1)2 sequence (a) and associated signal recovery (b): three look-locker inversion pulses are performed to acquire nine T₁-weighted images with a recovery period of one heartbeat between look-lockers. In MyoMapNet, images collected after the first look-locker are used for estimating the T₁ values.

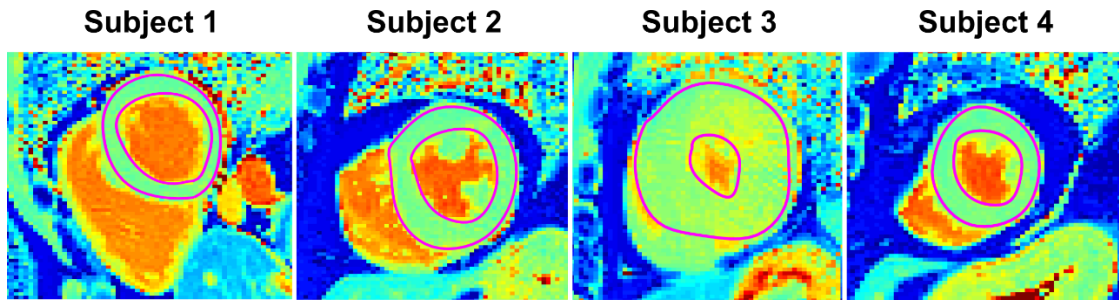


Figure S3. Example native T_1 maps with left ventricular myocardial segmentation used for analyzing T_1 estimations by MyoMapNet, MOLLI-5, and standard MOLLI-5(3)3.

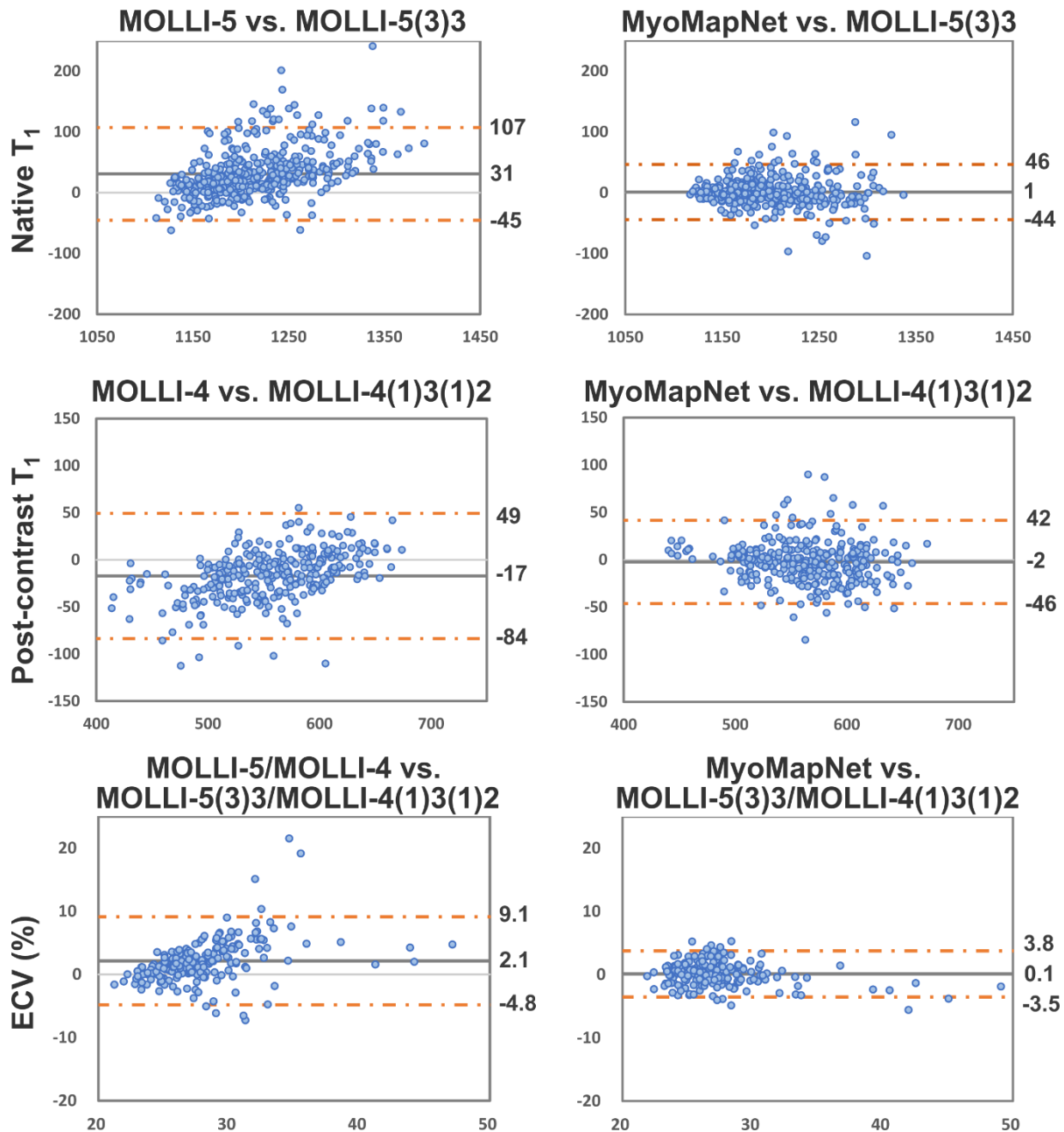


Figure S4. Bland-Altman plots showing per slice analysis of the mean difference and 95% limits of agreement for native, post-contrast T₁, and ECV for the abbreviated MOLLI-5/MOLLI-4 vs. standard MOLLI-5(3)3/MOLLI-4(1)3(1)2 (left column) and MyoMapNet vs. standard MOLLI-5(3)3/MOLLI-4(1)3(1)2 (right column). Each dot represents the values calculated from one slice.

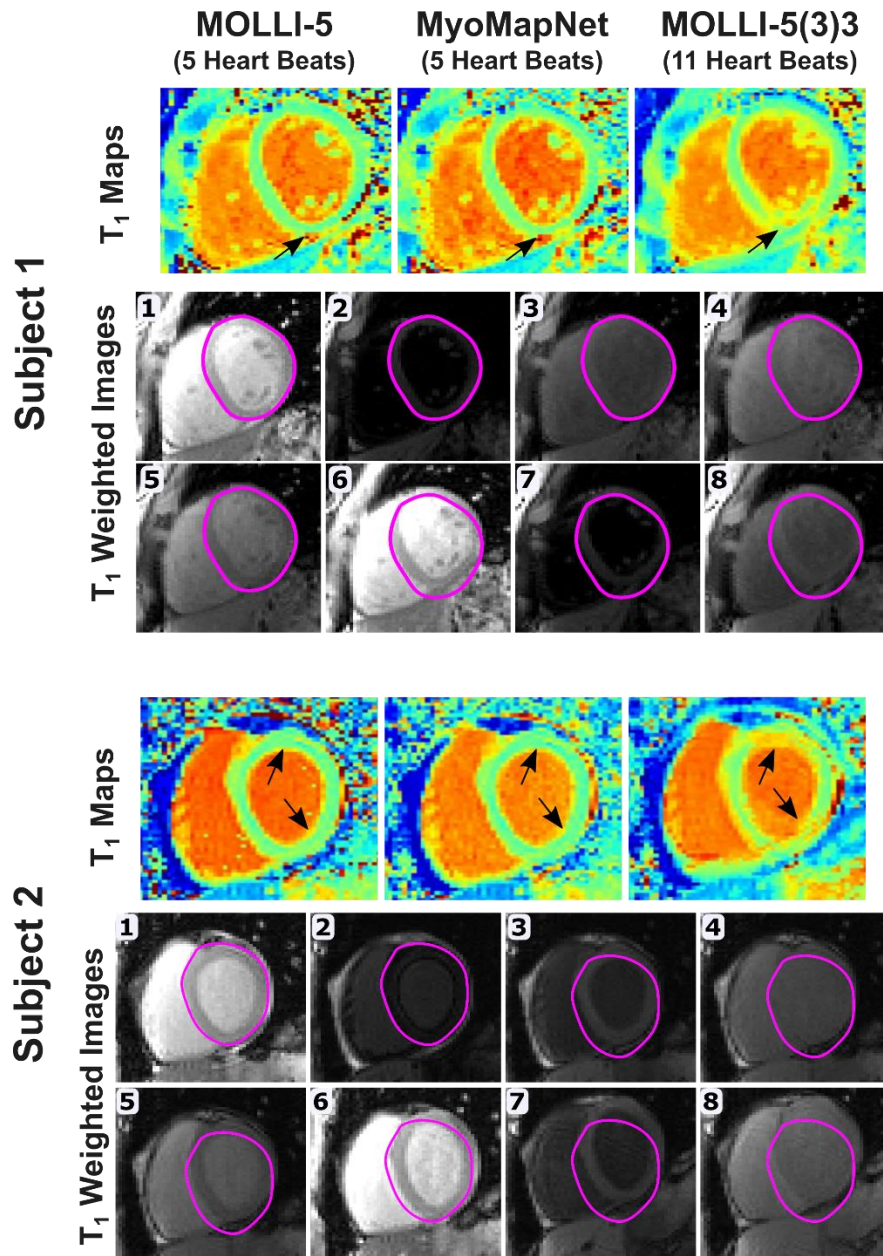


Figure S5. Myocardial T_1 maps calculated using MOLLI-5 with a 3-parameter fitting model, MyoMapNet, and MOLLI-5(3)3, demonstrating the impact of respiratory motion (black arrows) in two subjects. The epicardial delineation of image #1 was copied to all other T_1 -weighted images to show the degree of motion between images. Both subjects were instructed to hold their breath during the scan.